Combination Therapy with Anti–CTLA-4 and Anti–PD-1 Leads to Distinct Immunologic Changes In Vivo

Rituparna Das,[*,†] Rakesh Verma,[*,†] Mario Sznol,[*,†] Chandra Sekhar Boddupalli,[*,†] Scott N. Gettinger,[*,†] Harriet Kluger,[*,†] Margaret Callahan,[‡] Jedd D. Wolchok,[‡] Ruth Halaban,[§] Madhav V. Dhodapkar,[*,†] and Kavita M. Dhodapkar[*,†,¶]

Combination therapy concurrently targeting PD-1 and CTLA-4 immune checkpoints leads to remarkable antitumor effects. Although both PD-1 and CTLA-4 dampen the T cell activation, the in vivo effects of these drugs in humans remain to be clearly defined. To better understand biologic effects of therapy, we analyzed blood/tumor tissue from 45 patients undergoing single or combination immune checkpoint blockade. We show that blockade of CTLA-4, PD-1, or combination of the two leads to distinct genomic and functional signatures in vivo in purified human T cells and monocytes. Therapy-induced changes are more prominent in T cells than in monocytes and involve largely nonoverlapping changes in coding genes, including alternatively spliced transcripts and noncoding RNAs. Pathway analysis revealed that CTLA-4 blockade induces a proliferative signature predominantly in a subset of transitional memory T cells, whereas PD-1 blockade instead leads to changes in genes implicated in cytolysis and NK cell function. Combination blockade leads to nonoverlapping changes in gene expression, including proliferation-associated and chemokine genes. These therapies also have differential effects on plasma levels of CXCL10, soluble IL-2R, and IL-1α. Importantly, PD-1 receptor occupancy following anti–PD-1 therapy may be incomplete in the tumor T cells even in the setting of complete receptor occupancy in circulating T cells. These data demonstrate that, despite shared property of checkpoint blockade, Abs against PD-1, CTLA-4 alone, or in combination have distinct immunologic effects in vivo. Improved understanding of pharmacodynamic effects of these agents in patients will support rational development of immune-based combinations against cancer. ***The Journal of Immunology*****, 2015, 194: 950–959.**

Antigen-specific T cell activation is regulated by a balance of costimulatory and coinhibitory signals, such as those mediated by inhibitory receptors CTLA-4 and PD-1 (1). Abs that block these inhibitory receptors or their ligands such as PDL-1 have led to impressive antitumor effects in several cancers (2, 3). CTLA-4 blockade with Ipilimumab (Yervoy; Bristol-Myers Squibb, Princeton, NJ) was the first treatment demonstrated to improve survival of patients with stage IV melanoma in randomized trials (4). Clinical trials with anti–PD-1 Ab (such as Nivolumab) have demonstrated promising clinical activity in diverse tumor types, including melanoma, renal cell carcinoma, and lung cancer (5–8). In preclinical models, combined blockade of both PD-1 and CTLA-4 led to greater antitumor effects than either therapy alone, and, in a recent clinical trial, the combination of Nivolumab and Ipilimumab led to a distinct pattern of antitumor activity, with rapid and deep tumor regressions in a substantial proportion of melanoma patients (9, 10).

Clinical studies of PD-1 and CTLA-4 blockade in cancer patients have shown that the two therapies have clear differences in the frequency and pattern of immune-related adverse events (3, 11). Whereas the preclinical models of PD-1 or CTLA-4 blockade have to date been poorly predictive of the pattern of immune-related adverse events observed in the clinic, genetic deletion of PD-1 or CTLA-4 leads to very different effects in mice. CTLA-4 knockout mice suffer from a lethal lymphoproliferative disease, whereas deficiency of PD-1 leads to less severe phenotype with strain-specific autoimmunity (12–16). Although both PD-1 and CTLA-4 act to dampen T cell activation via shared signaling pathways, differences in sites of action have been proposed to help understand the differences in patterns of autoimmunity as well as antitumor effects with PD-1 and CTLA-4 blockade. For example, the effects of CTLA-4 may be mostly in lymphoid tissue, whereas PD-1 interactions may primarily occur in the periphery. Inhibitory signaling via both PD-1 and CTLA-4 in human T cells in culture was shown to converge on certain nodes such as inhibition of Akt phosphorylation, although the proximate events may differ, such as the involvement of phosphatase PP2A with CTLA-4, but not PD-1 (17–19). Improved understanding of the changes in gene expression in vivo in humans using genome-wide approaches in specific immune cells in response to checkpoint blockade therapy may provide new insights into the mechanisms of antitumor and autoimmune effects with these agents. In particular, it is important to understand whether combination checkpoint blockade in vivo leads to distinct or synergistic biologic effects compared with blockade of individual checkpoints in humans.

*Department of Medicine, Yale University School of Medicine, New Haven, CT 06520; †Smilow Cancer Center, Yale University School of Medicine, New Haven, CT 06520; ‡Ludwig Center for Cancer Immunotherapy, Memorial Sloan-Kettering Cancer Center, New York, NY 10065; §Department of Dermatology, Yale University School of Medicine, New Haven, CT 06520; and ¶Department of Pediatrics, Yale University School of Medicine, New Haven, CT 06520

Received for publication July 9, 2014. Accepted for publication November 18, 2014.

This work was supported in part by National Institutes of Health Grants RO1-AI0792222 (to K.M.D.), CA106802 (to M.V.D.), CA135110 (to M.V.D.), K24CA172123 (to H.K.), and P50-CA121974 (to R.H. and K.M.D.) and the Dana Foundation and Hyundai Hope on Wheels (to K.M.D.).

Address correspondence and reprint requests to Dr. Kavita M. Dhodapkar, Yale University School of Medicine, 333 Cedar Street, New Haven, CT 06520. E-mail address: kavita.dhodapkar@yale.edu

The online version of this article contains supplemental material.

Abbreviations used in this article: Combo, combination; Seq, sequential.

www.jimmunol.org/cgi/doi/10.4049/jimmunol.1401686

Materials and Methods

Patients

Peripheral blood and tumor tissue was obtained from patients (n = 45) undergoing immune checkpoint blockade after obtaining informed consent under a separate protocol for the collection of research samples approved by the Yale University Institutional Review Board. This included patients receiving anti–PD-1 (n = 24), anti–CTLA-4 (n = 9), or combination (Combo) therapy (n = 12; 9 concurrent, 3 sequential [Seq]).

Cell separation for gene expression analysis

PBMCs were obtained by density gradient centrifugation process using Ficoll Paque Plus (GE Health Care Life Sciences). Monocytes were sorted from PBMCs using anti-human CD14 microbeads (Miltenyi Biotec) using the manufacturer's protocol (20). Sample separation was performed using MACS-LS columns (Miltenyi Biotec). The $CD14^-$ fraction was further subjected to a second round of separation for T cells using Human *Pan* T Cell Isolation Kit I (Miltenyi Biotec). Purity of sorted populations was monitored by flow cytometry (Supplemental Fig. 1A). Monocytes and T cells obtained by MACS bead separation were pelleted, suspended in RLT buffer (Qiagen), and stored at −80°C for RNA isolation.

Gene expression analysis of purified monocytes and T cells

RNA was extracted from purified monocytes and T cells using the RNeasy Mini kit from Qiagen. We employed Affymetrix GeneChip Human Transcriptome 2.0 microarrays for gene expression profiling to allow analysis of coding as well as noncoding and alternatively spliced transcripts. Paired pretherapy and posttherapy samples from each patient for each cell type (monocyte or T cells) were compared directly to evaluate therapy-induced changes. We used Genespring GX 12.5 platform to analyze the changes in coding genes, exon workflow of the Partek GS 6.6 to analyze the alternatively spliced exons 2.0 genechip, as described by Whistler et al. (21, 22), and Partek GS 6.6 platform to analyze changes in the noncoding genes.

Analysis of coding genes

Data on coding genes were analyzed using Genespring GX 12.5 platform (20). Data were imported via exon expression workflow employing RMA16 or PLIER16 (normalization) for analyzing the coding genes using the specific annotation support file for human transcriptome array 2.0 (as provided by Genespring GX). Experiment grouping for each treatment cohort (anti–PD-1 alone, anti–CTLA-4 alone, concurrent anti–PD-1 + anti–CTLA-4; Combo and PD-1 following CTLA-4; Seq) was created for both T cells and monocytes, and interpretation for the posttreatment compared with pretreatment samples was generated. Quality control analysis was used in principal component analysis and for probe hybridization intensities. For the identification of the differentially regulated coding genes between post- and pretreatment samples for all treatment groups under each cell type, the locus filter was set on coding only genes (HTA gene chip 2.0 covers 44,699 genes/transcript clusters). We applied a t test with a p value cutoff set at 0.05, followed by the unsupervised clustering analysis using Genespring clustering workflow (Euclidean distance metric and Ward's linkage rule). Further statistical analysis involved application of a fold-change threshold of 1.3; differentially regulated genes were then manually curated to include coding genes only.

Pathway analysis

Pathway analysis of differentially expressed genes was performed using the Metacore pathway analysis platform (20). Differentially regulated gene lists with $p < 0.05$ and fold change of ±1.3 were used from each treatment group as input for the Metacore pathway platform, and differentially regulated pathways maps and gene ontology terms were generated.

Analysis of alternatively spliced genes

Analysis to detect the potentially alternatively spliced genes was performed using the Exon workflow of the Partek GS 6.6 by taking into account exon probes from Affymetrix HTA 2.0 genechip, as described by Whistler et al. (21, 22). Exons with a p value <0.05 were included for analysis. We obtained number of exon probe sets in each transcript cluster (with corresponding transcript cluster identification derived from the meta-probe set file) and discarded clusters with >100 probe sets or <10 probe sets and included exon clusters with alt-splice p value <0.00001. The list of alternatively spliced genes was filtered on gene clusters with p values <0.05 and a fold change of ±1.3 between pretherapy and posttherapy samples to obtain splice variants that were also differentially regulated at the gene level.

Analysis of noncoding genes

For analyzing the noncoding data, we used the Partek GS 6.6, postimporting data, and we employed the filter on noncoding genomic loci (22,829) to retain only the noncoding probe sets on the HTA 2.0 genechip from all samples. Statistical analysis involved one-way ANOVA, followed by application of a fold change threshold of 1.3 to generate noncoding transcript lists (unadjusted p value, 0.05). All the noncoding probe sets/transcript lists were further curated manually (via University of California Santa Cruz, Ensembl). Venn diagrams were generated between different treatment groups under each cell type.

Quantitative PCR

RNA from T cells isolated from patients pretherapy and posttherapy was used to validate the microarray data for the expression of Ki-67 and ICOS by quantitative PCR using the assays on demand primer probes (Applied Biosciences). Expression of GAPDH was monitored as a housekeeping gene. Reactions were set up in triplicates using EZ PCR Core reagents (Applied Biosciences), according to manufacturer's protocol. Relative expression of target genes was calculated using comparative threshold cycle method.

Immunoassay for detecting plasma levels of various cytokines

Plasma collected from patient samples before and after therapy (ipilimumab alone, n = 5; nivolumab alone, n = 20; concurrent ipilimumab + nivolumab [Combo], n = 6; and Seq nivolumab in patients with prior ipilimumab, n = 3) and stored at −20°C was thawed and used for the assay. Samples were used undiluted and in duplicate. Milliplex MAP Human Cytokine/Chemokine Magnetic Bead Panel Kit (MPXHCYTO-60K-PMX39; EMD Millipore) for 96-well plate assay was used for the simultaneous quantification of 39 human cytokines and chemokines (epidermal growth factor, eotaxin, fibroblast growth factor-2, Flt-3 ligand, fractalkine, G-CSF, GM-CSF, growth-related oncogene, IFN-α2, IFN-γ, IL-1α, IL-1β, IL-1rα, IL-2, IL-3, IL-4, IL-5, IL-6, IL-7, IL-8, IL-9, IL-10, IL-12 [p40], IL-12 [p70], IL-13, IL-15, IL-17A, IFN-γ–inducible protein-10, MCP-1, MCP-3, macrophage-derived chemokine, MIP-1α, MIP-1β, sCD40L, soluble IL-2Rα, TGF-α, TNF-α, TNF-β, vascular endothelial growth factor) using the protocol provided by the manufacturer. xPONENT software (Luminex) was used to detect, quantitate, and analyze the samples on the Luminex 100 instrument.

Detection of cytokines secreted by tumor-infiltrating T cells

Tumors were processed into single-cell suspension by manual dissociation and either left untreated or treated with anti-CD3/CD28 beads for 48 h in 96-well round-bottom plates in RPMI with 5% pooled human serum. Cell supernatant was collected at 48 h and analyzed for cytokines and chemokines using the Luminex assay, as described above.

Immunophenotyping of PBMCs

Cryopreserved patient presample and postsample PBMCs were thawed together and stained with dead cell exclusion dye and fluorochrome-conjugated anti-human Abs CD3, CD4, and CD8 (all from BD Pharmingen) and CD56 (BioLegend), CD25 (clone 4E3; Miltenyi Biotec), CD45RO (BD Horizon), as well as PD-1 (clone J105; eBioscience). For some samples, cells were fixed and permeabilized. After permeabilization of cells, fluorochrome-conjugated Abs against human granzyme B (BD Biosciences) and Ki-67 (eBioscience) were used to stain and detect the respective intracellular molecules. For detection of cytokine production, cells were rested overnight after thawing and then stimulated with PMA and ionomycin, both at 500 ng/ml in the presence of protein transport inhibitor BD Golgi Stop (0.7 μl/ml). After 5 h of stimulation, the cells were stained with the dead cell exclusion dye, fixed, permeabilized, and stained with fluorochrome-conjugated Abs against human CD3, CD4, CD8, and IFN-γ (all from BD Biosciences). All live cell stains were acquired on BD-LSR Fortessa, and the data were analyzed using Flowjo v9.7.5 software (Tree Star). Intracellular staining samples were acquired on BDLSR II, and the data analysis was done using Flowjo software.

Immunophenotyping by mass cytometry

Cryopreserved patient PBMCs were thawed in warm media containing Benzonase Nuclease (25 U/ml; Sigma-Aldrich) and washed twice. Pretherapy and posttherapy samples were thawed and stained at the same time. Cells were suspended at up to 10 million/ml in 1× PBS for viability staining by Cell-ID Cisplatin (final concentration of 5 μM; Fluidigm Sciences). Cells were mixed well and incubated for 5 min at room temperature. The staining was quenched with MaxPar Cell staining buffer and

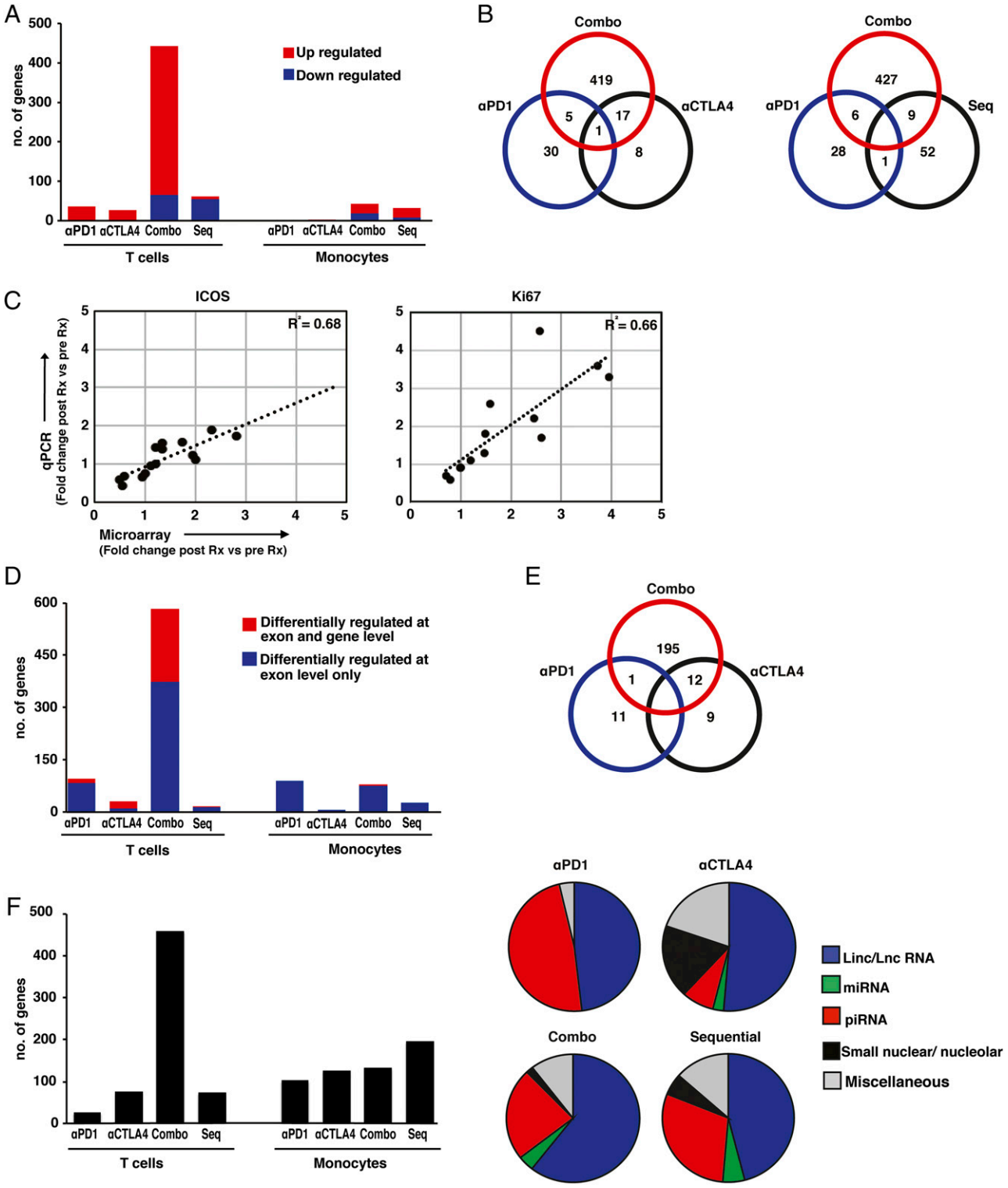

FIGURE 1. RNA extracted from freshly isolated monocytes and T cells from peripheral blood of patients treated with either anti–PD-1 (n = 6), anti–CTLA-4 (n = 5), Combo therapy with anti–PD-1 and anti–CTLA-4 concurrently (Combo, n = 6), and Seq anti–PD-1 in patients with prior anti–CTLA-4 (Seq, n = 3) was analyzed using the Affymetrix GeneChip Human Transcriptome 2.0 exon array. (**A**) The expression data for coding genes were analyzed using genespring 12.5platform. Coding genes were identified using the locus type filter on coding, followed by manual curation of the list obtained. Differentially regulated genes were obtained by using $p < 0.05$ and fold change $\pm$ 1.3-fold in posttherapy samples compared with pretherapy samples. Changes in expression of coding genes in peripheral blood T cells and monocytes of patients treated with anti–PD-1, anti–CTLA-4, Combo, or Seq therapy. Figure shows genes differently regulated ($p < 0.05$, fold change $\geq \pm 1.3$) in samples obtained 3 wk posttherapy compared with baseline prior to starting therapy. The genes that were upregulated are in red, and those that were downregulated are in blue. (**B**) Venn diagrams showing differentially regulated T cell coding genes that were shared between patients treated with anti–PD-1 (αPD1), anti–CTLA-4 (αCTLA4), Combo, and Seq therapy. The figure shows that majority of the genes were unique to each specific treatment group. (**C**) Quantitative PCR was performed to confirm expression of ICOS and Ki67, as determined by microarray (n = 15). Figure shows correlation between levels obtained by quantitative PCR versus expression levels as determined by gene array on the same patients. (**D**) Expression data were analyzed to detect alternatively spliced genes using exon flow workflow of *(Figure legend continues)*

Table I. Selected list of coding genes

Transcript ID	*p* Value	Fold Change	Gene Symbol	Gene Description
Combo therapy (anti–CTLA-4 + anti–PD-1)				
18876628	0.01	3.17	MKI67	Ag identified by mAb Ki-67
18906869	0.01	2.84	IFNG	IFN-γ
19224629	0.02	2.77	HIST1H3B	Histone cluster 1, H3b
18764511	0.05	2.77	IL8	IL-8
18775469	0.03	2.65	FGFBP2	Fibroblast growth factor binding protein 2
18772965	0.02	2.64	CCNA2	Cyclin A2
18949520	0.02	2.45	SLC7A5	Solute carrier family 7, member 5
18966489	0.001	2.39	KPNA2	Karyopherin α 2
18923230	0.04	2.29	GZMB	Granzyme B
18961872	0.02	2.13	TOP2A	Topoisomerase (DNA) II α, 170 kDa
Anti–CTLA-4 therapy				
18689122	0.021	2.33	FAM46C	Family with sequence similarity 46, member C
18876628	2.5E-04	2.18	MKI67	Ag identified by mAb Ki-67
18961872	0.002	1.59	TOP2A	Topoisomerase (DNA) II α, 170 kDa
18724103	0.035	1.58	CTLA-4	Cytotoxic T lymphocyte–associated protein 4
18797874	0.012	1.55	STX11	Syntaxin 11
19224662	0.003	1.54	HIST1H3F	Histone cluster 1, H3f
18772965	0.007	1.49	CCNA2	Cyclin A2
18906869	0.020	1.42	IFNG	IFN-γ
18988349	0.001	1.42	TPX2	TPX2 (microtubule associated)
18724111	0.06	1.57	ICOS*	Inducible T cell costimulator
Anti–PD-1 therapy				
18895449	0.028	2.67	KLRF1	Killer cell lectin-like receptor subfamily F, member 1
18707750	0.048	2.51	SH2D1B	SH2 domain containing 1B
18971449	0.027	2.23	KIR2DL2	Killer cell Ig-like receptor, two domains, long cytoplasmic tail, 2
18777270	0.021	2.07	GZMA	Granzyme A
18988173	0.013	1.97	CST7	Cystatin F (leukocystatin)
18718479	0.019	1.93	GNLY	Granulysin
18707252	0.004	1.77	FCRL3	FcR-like 3
19011576	0.025	1.60	HLA-DMA	MHC, class II, DM α
18978382	0.039	1.53	NCR1	Natural cytotoxicity triggering receptor 1
18906869	0.030	1.52	IFNG	IFN-γ
Seq therapy				
18896172	0.043	2.01	FAR2	Fatty acyl CoA reductase 2
18698492	0.010	1.46	PADI2	Peptidyl arginine deiminase, type II
19576522	0.008	1.43	ZFP57	Zinc finger protein 57 homolog (mouse)
18851261	0.000	1.35	IL3RA	IL-3R, α (low affinity)
18892472	0.030	1.35	CD3D	CD3D molecule, δ (CD3–TCR complex)
18968132	0.029	1.35	HRH4	Histamine receptor H4
18882589	0.007	1.34	FOLR3	Folate receptor 3 (γ)
18728884	0.031	−1.30	PRKD3	Protein kinase D3
18872598	0.021	−1.30	TIMM23	Translocase of inner mitochondrial membrane 23 homolog (yeast)
18891105	0.039	−1.30	RAB30	

Selected list of coding genes from the top 30 differentially regulated genes in T cells of patients treated with anti–CTLA-4, anti–PD-1, Combo therapy (concurrent anti–CTLA-4 and anti–PD-1), or Seq therapy (anti–PD-1 following anti–CTLA-4 therapy)

washed twice before proceeding to the usual procedure of surface and intracellular staining, as per manufacturer's protocol. MaxPar Human T Cell Phenotyping Panel Kit (CD11a-142Nd, CD4-145Nd, CD8a-146Nd, CD16-148Nd, CD25-149Sm, CD45-154Sm, CCR7-159Tb, CD69-162Dy, CD45RO-165Ho, CD44-166Er, CD27-167Er, CD45RA-169Tm, CD3-170Er, CD57-172Yb, HLA-DR-174Yb, and CD127-176Yb) was used along with CD28-160Gd (CD28.2), CD117-143Nd (104D2), and CD95-164Dy (DX2) for surface staining. Three million PBMCs were incubated in a volume of 100 μl cell staining buffer with Abs in a polystyrene tube for 30 min at room temperature. After staining, cells were washed twice with buffer before fixing with BD Cytofix fixation buffer (100 μl/million cells) and permeabilizing with BD Perm/Wash buffer. Fixed and permeabilized cells were stained with anti-human Ki-67-151Eu (B56; BD Pharmingen Ab conjugated with lanthanide MaxPar Europium Chloride 151Eu using the MaxPar X8 Ab labeling kit) for 30 min at room temperature. Cells were washed twice with buffer and suspended in 1 ml intercalation solution containing MaxPar Intercalator-Ir in MaxPar Fix and Perm buffer at final concentration of 125 nM. Cells were left overnight in the intercalator solution, washed with staining buffer, and finally suspended in 500 μl MaxPar Water before acquiring on CyTOF 2 instrument

Partek GS 6.6. Exons with probe sets between 10 and 100 and a *p* value of <0.05 at exon level and <0.00001 at the exon cluster level were included in the analysis. Figure shows alternatively spliced genes in peripheral T cells and monocytes of patients treated with anti–PD-1, anti–CTLA-4, Combo, and Seq therapy. Alternatively spliced genes differentially regulated at the exon level only are in blue, and genes differentially regulated at both the exon and gene level are represented in red. (**E**) Venn diagram showing differentially regulated alternatively spliced genes in T cells shared between patients treated with anti–PD-1, anti–CTLA-4, and Combo. (**F**) Expression data were analyzed for changes in noncoding genes using Partek GS 6.6. The bar graph shows noncoding genes that are differentially regulated ($p < 0.05$ and fold change of ± 1.3) in peripheral blood T cells and monocytes of patients receiving therapy with checkpoint blockade inhibitors. The pie charts show the type of noncoding genes (i.e., linc/LncRNA, miRNA, piRNA, etc.) that are differentially regulated in the T cells of the patients. Miscellaneous group includes antisense, transfer, ribosomal, and Y-RNA.

(DVS; Fluidigm Sciences). All data were analyzed and graphs generated using the DVS Cytobank software (Cytobank).

Results

To better understand the effects of Combo versus individual PD-1/CTLA-4 checkpoint blockade on human T cells and monocytes in vivo using a genome-wide approach, we initially analyzed gene expression profiles of purified $CD3^+$ T cells and $CD14^+$ monocytes in 20 patients before and 3 wk after receiving checkpoint blockade therapy with ipilimumab (anti–CTLA-4; $n = 5$), nivolumab (anti–PD-1; $n = 6$), concurrent ipilimumab and nivolumab (Combo; $n = 6$), or Seq nivolumab in patients with prior ipilimumab (Seq; $n = 3$) using an exon expression array (human HT2.0; Affymetrix). Therapy-induced changes in gene expression were analyzed utilizing baseline sample from each patient as its own control. Unsupervised cluster analysis revealed that the samples largely clustered according to pretherapy or posttherapy status, indicating that the impact of therapy was more dominant than the baseline variability between samples (Supplemental Fig. 1B). The use of exon expression array allowed us to examine changes in the expression of coding genes and splice variants as well as noncoding genes.

We first focused on therapy-induced changes in coding genes. Concurrent Combo therapy with both anti–CTLA-4 and anti–PD-1 led to greater number of differentially expressed T cell genes compared with either agent alone or both agents given sequentially (Combo = 442 genes; anti–CTLA-4 = 26 genes; anti–PD-1 = 36 genes; Seq anti–PD-1 in patients with prior anti–CTLA-4 = 62 genes) (Fig. 1A). Therapy-induced changes in gene expression included genes unique to each treatment cohort, including Combo therapy, with only minor overlap (Fig. 1B). The only upregulated gene shared between all three cohorts is IFN-γ. Interestingly, genomic changes following anti–PD-1 therapy showed little overlap with therapy-induced changes when anti–PD-1 therapy was applied as a Seq strategy in patients with prior anti–CTLA-4 therapy (Fig. 1B). Some of the notable genes induced in vivo following checkpoint blockade were Ki-67 (anti–CTLA-4 and Combo), granzyme A/B (anti–PD-1 and Combo), FCRL3 and KLRF1 (anti–PD-1), CTLA-4 and ICOS (anti–CTLA-4), IL-8 and HLA-DR (Combo), and IFN-γ (all three cohorts) (Table I). Data for changes in selected genes (ICOS and Ki67) were validated by quantitative PCR (Fig. 1C). In contrast to T cells, relatively few genes were differentially upregulated in monocytes following checkpoint blockade. This included increase in TNF following anti–CTLA-4 therapy.

Similar patterns emerged when exon level data were analyzed for evaluation of alternate splicing (Fig. 1D, 1E). The differentially spliced genes included both differentially regulated genes as well as genes that were not differentially regulated with therapy. The proportion of genes with altered exon usage that were also differentially regulated at the gene level was 34% with Combo therapy, 67% with anti–CTLA-4, 13% with anti–PD-1 therapy, and 7% with Seq therapy. The sites of altered exon usage were similar for genes shared between CTLA-4– and Combo-treated patients (data not shown). Similar to the pattern with the coding genes, Combo therapy led to greatest changes in noncoding genes in T cells. Majority of the changes in noncoding genes in T cells were observed in long noncoding RNAs and piwi RNAs (Fig. 1F), and there was little overlap between differentially regulated noncoding genes between the three treatment groups (data not shown). Together these data demonstrate that each of the checkpoint blockade strategies leads to distinct and largely nonoverlapping effects on the transcriptome of human T cells in vivo.

Pathway analysis of differentially expressed coding transcripts revealed that the dominant pathway in the setting of CTLA-4 blockade and Combo therapy was cell cycle/proliferation (Table II). In contrast to CTLA-4/Combo blockade, PD-1-regulated genes did not include a proliferation signature and were instead enriched for genes implicated in cytolytic function and regulation of effector T and NK cell function.

Next, we analyzed the expression of Ki-67 and granzyme in T cells by flow cytometry, as these represented two distinct aspects of T cell function (proliferation and cytolytic function) that appear to be the major functional pathways differentially activated by CTLA-4 and PD-1 blockade, respectively, in vivo in human T cells. Flow cytometry of paired pretherapy and posttherapy samples

Table II. Metacore pathway analysis

	Pathway	p Value (FDR)
Anti–PD-1 therapy		
1	Immune response: role of DAP12 receptors in NK cells	2.2E-13
2	Immune response: T regulatory cell–mediated modulation of effector T and NK cell functions	8.5E-03
3	Immune response: IL-27 signaling pathway	1.9E-02
4	Immune response: IL-12–induced IFN-γ production	4.2E-02
5	Immune response: differentiation and clonal expansion of $CD8^+$ T cells	4.2E-02
Anti–CTLA-4 therapy		
1	Cell cycle: transition and termination of DNA replication	5.5E-03
2	Cell cycle: spindle assembly and chromosome separation	5.5E-03
3	Cell cycle: nucleocytoplasmic transport of CDK/cyclins	2.4E-02
4	Cell cycle: chromosome condensation in prometaphase	3.0E-02
Combo therapy (PD-1 + CTLA-4)		
1	Cell cycle: chromosome condensation in prometaphase	6.4E-04
2	DNA damage: ATM/ATR regulation of G_1/S checkpoint	1.4E-06
3	DNA damage: ATM/ATR regulation of G_2/M checkpoint	1.4E-06
4	Cell cycle: transition and termination of DNA replication	1.4E-06
10	Immune response: differentiation and clonal expansion of $CD8^+$ T cells	0.059
Seq therapy		
1	Immune response: T regulatory cell–mediated modulation of effector T and NK cell functions	3.7E-02
2	Apoptosis and survival: endoplasmic reticulum stress response pathway	4.3E-02

Metacore pathway analysis was used to analyze coding genes that were differentially regulated ($p < 0.05$, fold change ± 1.3) between pretherapy and posttherapy T cells obtained from patients treated with either anti–PD-1 alone or anti–CTLA-4 alone, as well as anti–CTLA-4 and anti–PD-1 in Combo either concurrently (Combo therapy) or sequentially (Seq therapy). Table shows pathways that were differentially regulated in each group.

ATM/ATR, ataxia-telangiectasia mutated/ataxia-telangiectasia mutated and Rad3-related; CDK, cyclin-dependent kinase; FDR, false discovery rate

(n = 34 patients) confirmed the microarray data for the induction of Ki-67 following Combo and CTLA-4 blockade. Ki67 was induced after therapy with anti–CTLA-4 or Combo in both CD4 and CD8 T cells (Fig. 2A), and the Ki67$^+$ cells had a CD45RO$^+$ memory phenotype (Fig. 2B). To further dissect the phenotype of Ki-67$^+$ cells following checkpoint blockade, these cells were analyzed by single-cell mass cytometry. The data revealed that the Ki-67$^+$ cells increasing after Combo checkpoint blockade have a phenotype of CD45RO$^+$, CCR7$^-$CD27$^+$CD28$^+$CD95$^+$, consistent with transitional memory T cells (Fig. 2C) (23). The proliferating cells upregulated HLA-DR. Anti–PD-1 as well as Combo therapy led to an increase in granzyme B, whereas this was not observed in the cohort that received anti–CTLA-4 or Seq therapy (Fig. 2D). Together these data demonstrate that each of the therapeutic approaches at immune checkpoint blockade leads to a distinct, but largely nonoverlapping signature of changes in gene expression in T cells in vivo, which represent distinct aspects of T cell function and can be readily detected in freshly isolated circulating immune cells.

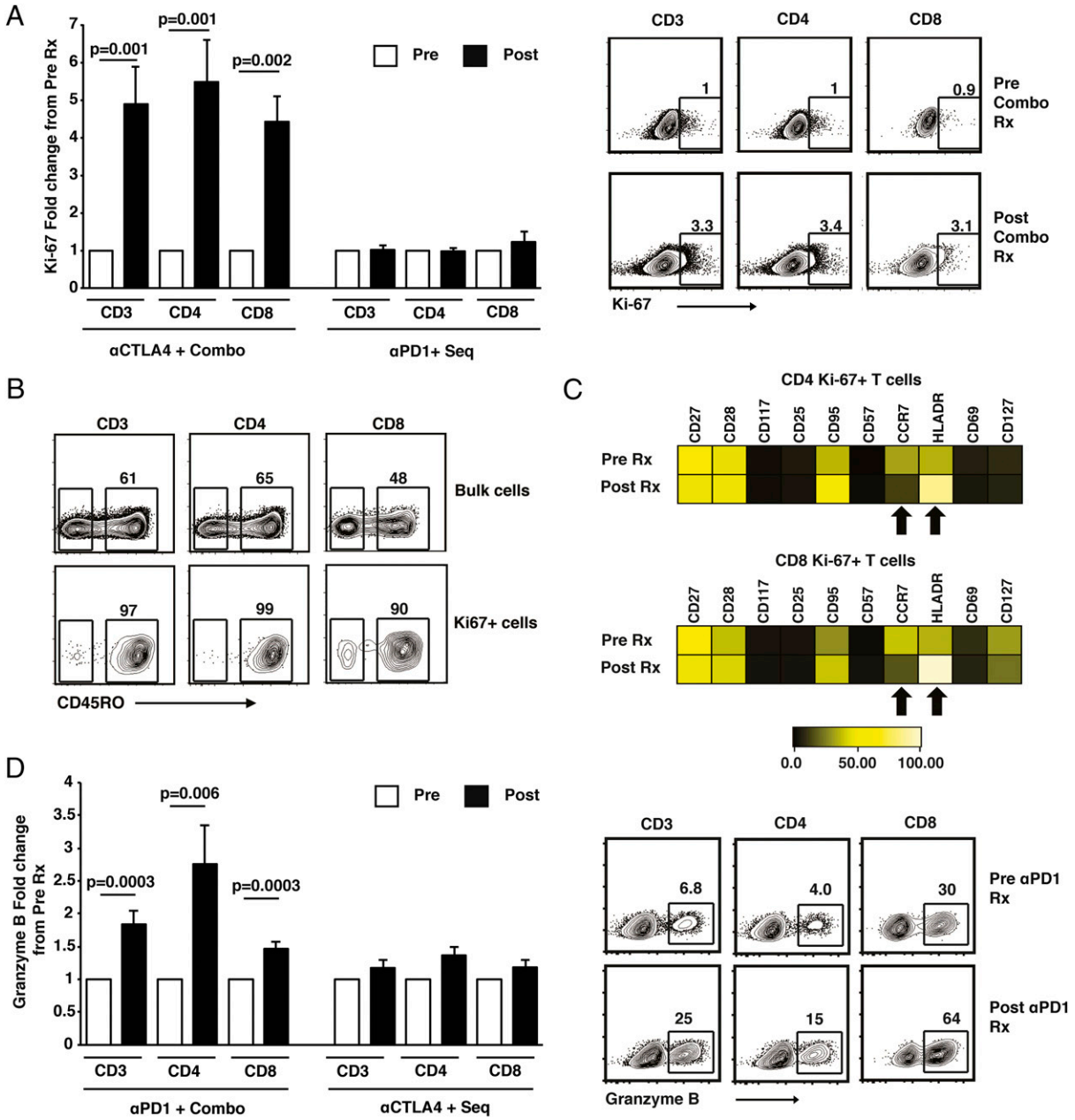

FIGURE 2. Changes in T cell proliferation and cytolytic function following therapy with checkpoint blockade inhibitors. Freshly collected frozen samples were used for these assays. All pretherapy and posttherapy samples from the same patient were thawed at the same time, stained together using the same Ab mixture, and analyzed at the same time. (**A**) Bar graph shows expression of Ki67 (mean and SEM) in peripheral blood (CD3, CD4, and CD8 T cells) of patients (n = 34) before (Pre, white bars) and after (Post, black bars) therapy with either anti–CTLA-4 and Combo therapy (n = 15) or anti–PD-1 and Seq therapy (n = 19). Flow cytometry plots on the *right* show a representative patient with increase in Ki67$^+$ cells after Combo therapy. (**B**) Expression of T cell memory marker (CD45RO) in bulk T cells as well as Ki67-positive T cells after therapy in the same patient as in (A). (**C**) Single-cell mass cytometry (CyTOF) analysis for expression of surface markers on CD3$^+$CD4$^+$ Ki67$^+$ as well as CD3$^+$CD8$^+$ Ki67$^+$ cells before (Pre Rx) and 3 wk after (Post Rx) starting Combo therapy with anti–CTLA-4 and anti–PD-1. The figure shows median mean fluorescence intensity. Plot is representative of three similar patients (anti–CTLA-4 = 2, and Combo-treated patients, n = 1). (**D**) Expression of granzyme B (mean and SEM) in CD3 and CD8 T cells in peripheral blood of patients (n = 34) before (Pre) and after (Post) therapy with anti–PD-1 and Combo therapy (Combo; n = 23) and those treated with anti–CTLA-4 and Seq therapy (n = 11). The flow cytometry plot shows a representative patient.

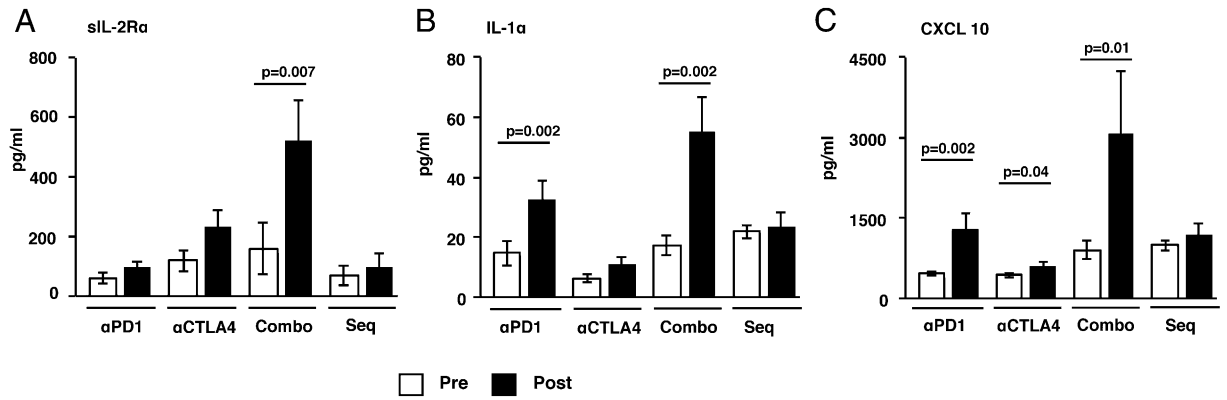

FIGURE 3. Changes in plasma chemokine and cytokines of patients treated with checkpoint blockade inhibitors. Plasma collected before and after therapy with anti–PD-1, anti–CTLA-4, Combo therapy, as well as Seq therapy was analyzed for presence of cytokines and chemokines using 39-plex luminex assay. All samples were tested in duplicate. Figure shows data for levels of cytokines and chemokines (mean and SEM) that were differentially secreted. (**A**) sIL-2Rα levels, (**B**) IL-1α levels, and (**C**) CXCL10/IP10 levels in plasma of patients pretherapy and posttherapy.

As checkpoint blockade therapy led to changes that were detected in circulating immune cells, we hypothesized that these therapies would also lead to detectable changes in systemic levels of cytokines. Accordingly, we evaluated changes in the plasma levels of a panel of 39 cytokines/chemokines/growth factors before/after therapy in these patients using Luminex analysis. Of the analytes tested, soluble IL-2R was increased following Combo therapy, whereas the levels of IL-1α were increased following anti–PD-1 and Combo blockade, and CXCL10 levels were increased following anti–PD-1, anti–CTLA-4, and Combo blockade (Fig. 3). Together these data demonstrate that each form of immune checkpoint blockade is associated with a distinct pattern of systemic changes in cytokines.

In contrast to single-agent CTLA-4 or PD-1 blockade, less is known about the effects of Combo checkpoint blockade on T cells infiltrating human tumors. An impressive aspect of such therapy is the rapidity and depth of clinical response. Therefore, to characterize early changes in tumor-infiltrating immune T cell function following such therapy, we analyzed serial biopsies before and after initiation of therapy in a patient treated with Combo checkpoint blockade. When compared with baseline, freshly isolated tumor-infiltrating T cells from just 3 wk posttherapy demonstrated increased production of IFN-γ, indicating rapid induction of effector T cell function in the tumor bed (Fig. 4A, 4B). Analysis of circulating T cells obtained at the same time as the tumor biopsies also showed an increase in IFN-γ^+ T cells following Combo therapy, indicating that these early changes are also detectable in the peripheral blood (Fig. 4C).

Current dosing strategies for Nivolumab in the clinic have been guided by prior studies demonstrating that doses of Nivolumab as low as 1 mg/kg lead to complete saturation of PD-1 receptor on circulating T cells (8). As in prior studies, tumor-infiltrating T cells expressed higher levels of PD-1 on their surface compared with peripheral blood T cells (Fig. 5A). Interestingly, surface staining for PD-1 (clone J105; eBioscience) was abrogated in circulating T cells from patients treated with anti–PD-1 Ab, but not in those treated with anti–CTLA-4 Ab, consistent with treatment-specific staining interference likely due to receptor occupancy in vivo following anti–PD-1 therapy (8) (Fig. 5B). However, at least in two patients with available biopsies before and after therapy with anti–PD-1 (either alone or in Combo with CTLA-4), the blockade of PD-1 on tumor-infiltrating lymphocytes was incomplete, even in the setting of complete blockade of PD-1 on both CD4 and CD8 T cells in the circulation (Fig. 5C, 5D).

Discussion

To our knowledge, these studies provide the first comparison of in vivo changes in purified human immune cells following Combo checkpoint blockade versus individual CTLA-4 or PD-1 checkpoint blockade in human cancer. An important aspect of this study

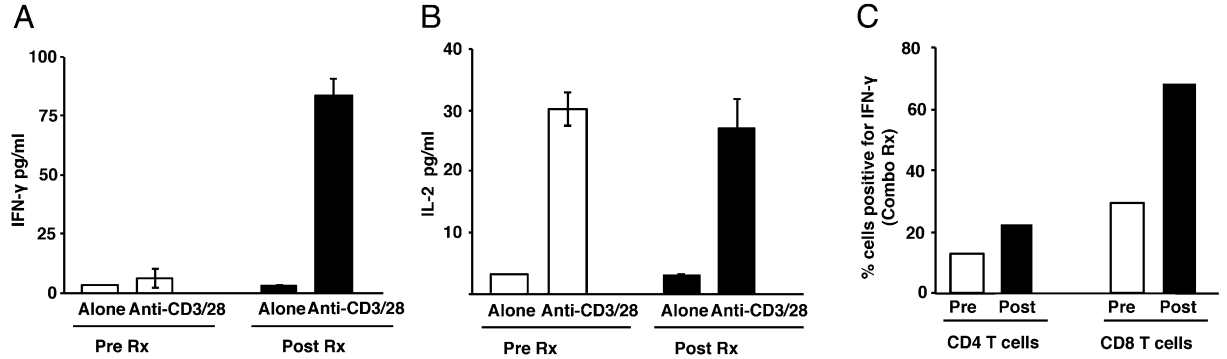

FIGURE 4. Early effects of Combo blockade on cytokine secretion by tumor-infiltrating lymphocytes. Tumor biopsy and peripheral blood were obtained from a patient before and 3 wk after starting Combo therapy with ipilimumab and nivolumab. Tumor-infiltrating lymphocytes were either cultured alone (Alone) or with anti-CD3/CD28 beads (Anti-CD3/28). Culture supernatant obtained at 48 h was subjected to luminex assay. PBMCs obtained at the same time were stimulated with PMA and ionomycin, and intracellular flow cytometry was performed for the detection of IFN-γ. (**A**) Secretion of IFN-γ by tumor-infiltrating lymphocytes before and after therapy. (**B**) Secretion of IL-2 by the tumor-infiltrating lymphocytes. (**C**) Percentage of IFN-γ–positive CD4 and CD8 T cells in the peripheral blood obtained pretherapy and posttherapy from the same patient.

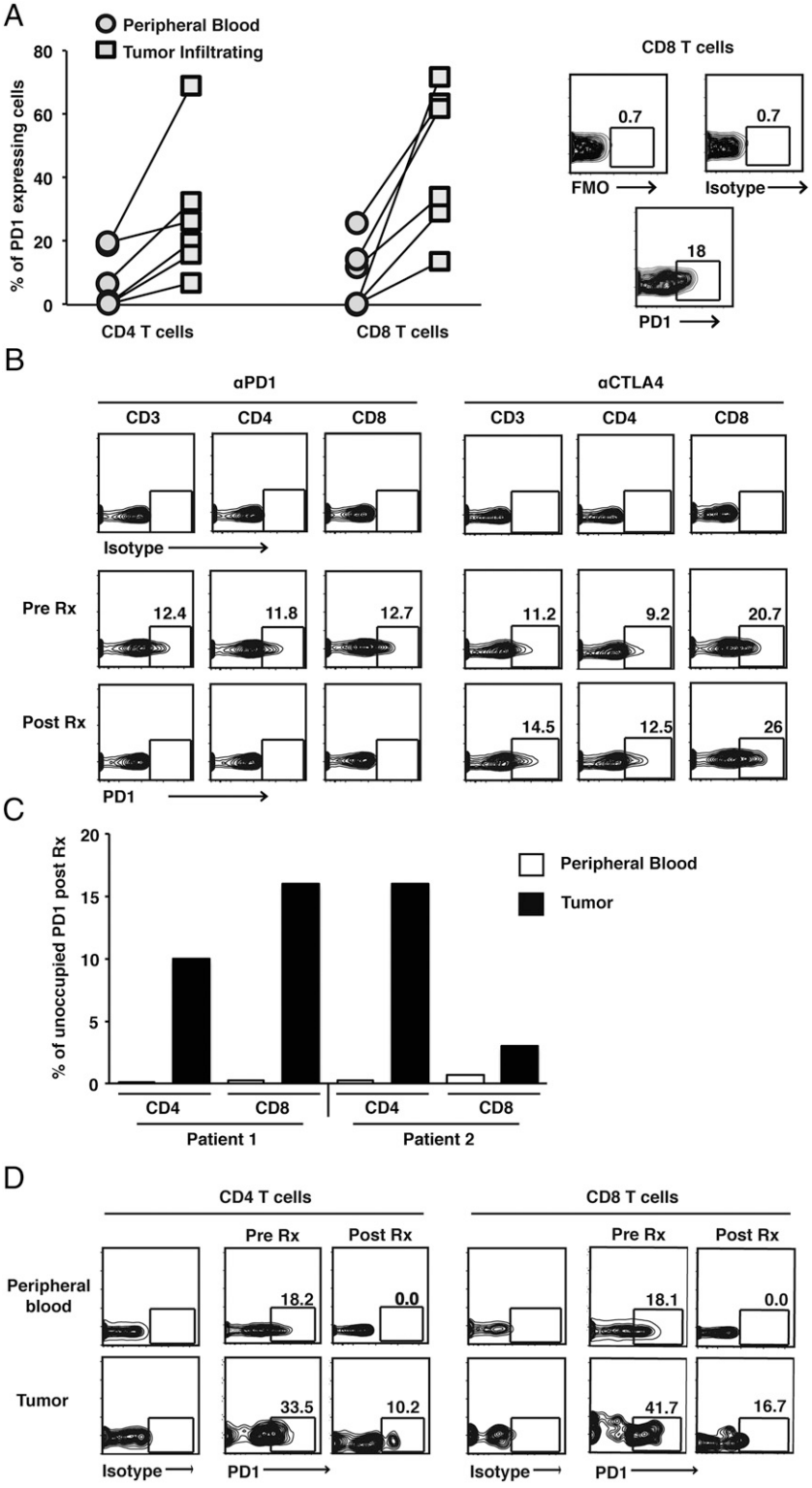

FIGURE 5. PD-1 expression and occupancy in patients treated with checkpoint blockade inhibitors. PD-1 surface expression was determined on tumor-infiltrating lymphocytes and blood from patients (n = 6 different patients). Cells were obtained from the tumor sample by manual dissociation. PBMCs obtained from the blood and the tumor tissue were stained and analyzed together. (**A**) Graph in the *left panel* shows expression of PD-1 on CD4 and CD8 T cells in the tumor as well as peripheral blood T cells drawn at the same time. Panel on the *right* is a representative flow cytometry plot showing controls (fluorescence minus one [FMO] and isotype) as well as PD-1 staining on CD8 T cells. (**B**) Expression of PD-1 on CD3, CD4, and CD8 T cells in peripheral blood of representative patients before and after treatment with anti–PD-1 and anti–CTLA-4. (**C**) Bar graph shows percentage of PD-1 on CD4 and CD8 T cells that was unoccupied after therapy with anti–PD-1 compared with that prior to therapy in two separate patients. Bar in white shows data from peripheral blood T cells, and bar in black shows data from tumor-infiltrating T cells. (**D**) Expression of PD-1 on peripheral blood and tumor-infiltrating T cells in a patient before and after Combo therapy with anti–CTLA-4 and anti–PD-1 therapy. Data are representative of similar findings on two patients.

is that the changes in gene expression were analyzed in highly purified immune cells and that both T cells and monocytes were purified from fresh blood mononuclear cells immediately after blood draw, without a potential artifact of in vitro culture, shipping, or cryopreservation. The data clearly demonstrate that the effects of CTLA-4, PD-1, or Combo blockade can be readily detected in circulating T cells, and that each therapy leads to distinct patterns of immune activation in vivo, despite known convergence of signaling pathways downstream of the inhibitory receptors (17). Notably, the effects of Combo blockade are distinct from that of individual checkpoints, which may help the differences in clinical effects of these therapies.

These findings have several potential implications for understanding the antitumor and autoimmune effects observed with these therapies in the clinic and the development of new Combos. Although CTLA-4 blockade induces a robust proliferation signature in T cells, this was not observed following PD-1 blockade, indicating that the two modes of checkpoint blockade therapies have very different effects on human T cells in vivo. In contrast to CTLA-4, PD-1 blockade is associated with the induction of several

cytolysis and NK-associated genes. For example, in addition to the well-documented roles of granzyme and granulysin, majority of the top PD-1–regulated genes such as cystatin F and CD244 have also been implicated in the regulation of lytic function or secretory granules (24–27). The finding that PD-1 blockade particularly leads to the expression of several NK-associated genes on T cells should encourage further exploration of the possible effects of PD-1 blockade on NKT cells as well as Combos targeting innate cells with PD-1 blockade (28–30). Genomic signature of CTLA-4 blockade includes the induction of several cell cycle–associated genes, best exemplified by upregulation of Ki-67 on a subset of transitional memory T cells, which is consistent with preclinical studies showing CTLA-4–mediated dampening of proliferation and enhanced memory following CTLA-4 blockade in mice (31–33). It is notable that the CTLA-4–regulated genes (such as Ki-67) described in this study bear a strong similarity to findings in another study analyzing changes in gene expression in purified T cells postipilimumab with a different gene expression profiling platform, which provides additional validation for our findings (34). To our knowledge, this is the first study to compare gene expression profiling of purified immune cells in vivo following Combo and PD-1 blockade therapies. In contrast to single-agent therapies, Combo therapy leads to the induction of much larger number of genes, involving greater increase in genes induced by single agents, but also distinct genes observed only with Combo blockade. Interestingly, the latter set of genes includes potent chemokines (such as IL-8), which may increase immune infiltration and may help explain why the clinical response to the Combo therapy was found to be independent of pre-existing immune infiltration and PDL-1 expression in the tumor (9, 10).

In addition to the coding genes, we also identified differential regulation of several noncoding genes as well as altered exon splicing. Most of these have not yet been studied in the context of human immune system, although the importance of RNA splicing and noncoding RNAs in immune regulation is increasingly appreciated. It is notable that some of the coding as well as noncoding genes (such as linc RNAs) identified in this work have prominent species-specific effects, imploring the need to directly study patients treated with these agents. For example, FCRL3 induced following PD-1 blockade is a human-specific T/NK-associated gene strongly implicated by genetic studies in human autoimmunity (35, 36). In contrast to some prior studies, purification of immune cells allowed us to specifically study genomic changes in T cells and monocytes (37). Although the immune signatures that we observed are quite robust, one of the limitations of this study is the small numbers of patients studied. Further studies with additional patients are needed to better understand the correlation between genomic signatures and other aspects of immune response with clinical outcome following checkpoint blockade (8, 38).

These data may also have possible implications for optimal management of therapy-induced autoimmunity. Currently, immune-related adverse events following checkpoint blockade are clinically managed with steroids, with TNF blockade reserved for refractory cases. The use of TNF blockade in severe colitis associated with CTLA-4 blockade is also supported by our finding of TNF as the top differentially regulated gene in myeloid cells of anti–CTLA-4–treated patients (39). However, differences in genomic and cytokine profiles following CTLA-4 and PD-1 blockade as shown in this work raise the possibility that optimal management of autoimmune events in the two settings may differ. For example, the finding that PD-1 (but not CTLA-4) blockade leads to an increase in plasma IL-1α suggests that some cases of PD-1–induced autoinflammation may benefit from consideration of such an IL-1 blockade already in the clinic, but yet unexplored in this setting (40).

Recent clinical success of PD-1/CTLA-4 Combo therapy has led to much excitement in cancer immunotherapy (10). When designing this Combo, the dose of anti–PD-1 was not escalated beyond 3 mg/kg, due to dose-limiting toxicity and prior data about saturation of the receptor in circulating T cells at much lower doses (8, 10). Our data demonstrate that such a strategy might need to be re-evaluated, and monitoring changes in tumor-infiltrating lymphocytes including receptor occupancy in individual patients may allow for optimal dosing of anti–PD-1 Ab as a part of the Combo. Optimal development of checkpoint blockade Combos in the clinic will require careful evaluation of pharmacodynamics effects in the tumor bed in patients undergoing these Combo therapies.

Acknowledgments

We acknowledge Matthew Burke and Antonella Bacchiocchi for help with patient consents and sample collection, Anumeha Shah and Lin Zhang for technical support, and Xiting Yan for help with pathway analysis.

Disclosures

M.S. received consulting fees from Bristol-Myers Squibb. M.C. received research funding from Bristol-Myers Squibb. J.D.W. received consulting fees as well as research funding from Bristol-Myers Squibb. The other authors have no financial conflicts of interest.

References

1. Krummel, M. F., and J. P. Allison. 1995. CD28 and CTLA-4 have opposing effects on the response of T cells to stimulation. *J. Exp. Med.* 182: 459–465.
2. Pardoll, D. M. 2012. The blockade of immune checkpoints in cancer immunotherapy. *Nat. Rev. Cancer* 12: 252–264.
3. Sznol, M., and L. Chen. 2013. Antagonist antibodies to PD-1 and B7-H1 (PD-L1) in the treatment of advanced human cancer. *Clin. Cancer Res.* 19: 1021–1034.
4. Hodi, F. S., S. J. O'Day, D. F. McDermott, R. W. Weber, J. A. Sosman, J. B. Haanen, R. Gonzalez, C. Robert, D. Schadendorf, J. C. Hassel, et al. 2010. Improved survival with ipilimumab in patients with metastatic melanoma. *N. Engl. J. Med.* 363: 711–723.
5. Hamid, O., C. Robert, A. Daud, F. S. Hodi, W. J. Hwu, R. Kefford, J. D. Wolchok, P. Hersey, R. W. Joseph, J. S. Weber, et al. 2013. Safety and tumor responses with lambrolizumab (anti-PD-1) in melanoma. *N. Engl. J. Med.* 369: 134–144.
6. Topalian, S. L., M. Sznol, D. F. McDermott, H. M. Kluger, R. D. Carvajal, W. H. Sharfman, J. R. Brahmer, D. P. Lawrence, M. B. Atkins, J. D. Powderly, et al. 2014. Survival, durable tumor remission, and long-term safety in patients with advanced melanoma receiving nivolumab. *J. Clin. Oncol.* 32: 1020–1030.
7. Brahmer, J. R., S. S. Tykodi, L. Q. Chow, W. J. Hwu, S. L. Topalian, P. Hwu, C. G. Drake, L. H. Camacho, J. Kauh, K. Odunsi, et al. 2012. Safety and activity of anti-PD-L1 antibody in patients with advanced cancer. *N. Engl. J. Med.* 366: 2455–2465.
8. Topalian, S. L., F. S. Hodi, J. R. Brahmer, S. N. Gettinger, D. C. Smith, D. F. McDermott, J. D. Powderly, R. D. Carvajal, J. A. Sosman, M. B. Atkins, et al. 2012. Safety, activity, and immune correlates of anti-PD-1 antibody in cancer. *N. Engl. J. Med.* 366: 2443–2454.
9. Curran, M. A., W. Montalvo, H. Yagita, and J. P. Allison. 2010. PD-1 and CTLA-4 combination blockade expands infiltrating T cells and reduces regulatory T and myeloid cells within B16 melanoma tumors. *Proc. Natl. Acad. Sci. USA* 107: 4275–4280.
10. Wolchok, J. D., H. Kluger, M. K. Callahan, M. A. Postow, N. A. Rizvi, A. M. Lesokhin, N. H. Segal, C. E. Ariyan, R. A. Gordon, K. Reed, et al. 2013. Nivolumab plus ipilimumab in advanced melanoma. *N. Engl. J. Med.* 369: 122–133.
11. Page, D. B., M. A. Postow, M. K. Callahan, J. P. Allison, and J. D. Wolchok. 2014. Immune modulation in cancer with antibodies. *Annu. Rev. Med.* 65: 185–202.
12. Chambers, C. A., T. J. Sullivan, and J. P. Allison. 1997. Lymphoproliferation in CTLA-4-deficient mice is mediated by costimulation-dependent activation of CD4+ T cells. *Immunity* 7: 885–895.
13. Waterhouse, P., J. M. Penninger, E. Timms, A. Wakeham, A. Shahinian, K. P. Lee, C. B. Thompson, H. Griesser, and T. W. Mak. 1995. Lymphoproliferative disorders with early lethality in mice deficient in Ctla-4. *Science* 270: 985–988.
14. Nishimura, H., N. Minato, T. Nakano, and T. Honjo. 1998. Immunological studies on PD-1 deficient mice: implication of PD-1 as a negative regulator for B cell responses. *Int. Immunol.* 10: 1563–1572.
15. Tivol, E. A., F. Borriello, A. N. Schweitzer, W. P. Lynch, J. A. Bluestone, and A. H. Sharpe. 1995. Loss of CTLA-4 leads to massive lymphoproliferation and fatal multiorgan tissue destruction, revealing a critical negative regulatory role of CTLA-4. *Immunity* 3: 541–547.

16. Nishimura, H., T. Okazaki, Y. Tanaka, K. Nakatani, M. Hara, A. Matsumori, S. Sasayama, A. Mizoguchi, H. Hiai, N. Minato, and T. Honjo. 2001. Autoimmune dilated cardiomyopathy in PD-1 receptor-deficient mice. *Science* 291: 319–322.
17. Parry, R. V., J. M. Chemnitz, K. A. Frauwirth, A. R. Lanfranco, I. Braunstein, S. V. Kobayashi, P. S. Linsley, C. B. Thompson, and J. L. Riley. 2005. CTLA-4 and PD-1 receptors inhibit T-cell activation by distinct mechanisms. *Mol. Cell. Biol.* 25: 9543–9553.
18. Riley, J. L., M. Mao, S. Kobayashi, M. Biery, J. Burchard, G. Cavet, B. P. Gregson, C. H. June, and P. S. Linsley. 2002. Modulation of TCR-induced transcriptional profiles by ligation of CD28, ICOS, and CTLA-4 receptors. *Proc. Natl. Acad. Sci. USA* 99: 11790–11795.
19. Okazaki, T., A. Maeda, H. Nishimura, T. Kurosaki, and T. Honjo. 2001. PD-1 immunoreceptor inhibits B cell receptor-mediated signaling by recruiting src homology 2-domain-containing tyrosine phosphatase 2 to phosphotyrosine. *Proc. Natl. Acad. Sci. USA* 98: 13866–13871.
20. Sehgal, K., X. Guo, S. Koduru, A. Shah, A. Lin, X. Yan, and K. M. Dhodapkar. 2013. Plasmacytoid dendritic cells, interferon signaling, and FcγR contribute to pathogenesis and therapeutic response in childhood immune thrombocytopenia. *Sci. Transl. Med.* 5: 93ra89.
21. Furney, S. J., M. Pedersen, D. Gentien, A. G. Dumont, A. Rapinat, L. Desjardins, S. Turajlic, S. Piperno-Neumann, P. de la Grange, S. Roman-Roman, et al. 2013. SF3B1 mutations are associated with alternative splicing in uveal melanoma. *Cancer Discov.* 3: 1122–1129.
22. Whistler, T., C. F. Chiang, W. Lonergan, M. Hollier, and E. R. Unger. 2010. Implementation of exon arrays: alternative splicing during T-cell proliferation as determined by whole genome analysis. *BMC Genomics* 11: 496.
23. Fritsch, R. D., X. Shen, G. P. Sims, K. S. Hathcock, R. J. Hodes, and P. E. Lipsky. 2005. Stepwise differentiation of CD4 memory T cells defined by expression of CCR7 and CD27. *J. Immunol.* 175: 6489–6497.
24. Sivori, S., S. Parolini, M. Falco, E. Marcenaro, R. Biassoni, C. Bottino, L. Moretta, and A. Moretta. 2000. 2B4 functions as a co-receptor in human NK cell activation. *Eur. J. Immunol.* 30: 787–793.
25. Hamilton, G., J. D. Colbert, A. W. Schuettelkopf, and C. Watts. 2008. Cystatin F is a cathepsin C-directed protease inhibitor regulated by proteolysis. *EMBO J.* 27: 499–508.
26. Clark, R., and G. M. Griffiths. 2003. Lytic granules, secretory lysosomes and disease. *Curr. Opin. Immunol.* 15: 516–521.
27. Lieberman, J. 2003. The ABCs of granule-mediated cytotoxicity: new weapons in the arsenal. *Nat. Rev. Immunol.* 3: 361–370.
28. Parekh, V. V., S. Lalani, S. Kim, R. Halder, M. Azuma, H. Yagita, V. Kumar, L. Wu, and L. V. Kaer. 2009. PD-1/PD-L blockade prevents anergy induction and enhances the anti-tumor activities of glycolipid-activated invariant NKT cells. *J. Immunol.* 182: 2816–2826.
29. Benson, D. M., Jr., C. E. Bakan, A. Mishra, C. C. Hofmeister, Y. Efebera, B. Becknell, R. A. Baiocchi, J. Zhang, J. Yu, M. K. Smith, et al. 2010. The PD-1/PD-L1 axis modulates the natural killer cell versus multiple myeloma effect: a therapeutic target for CT-011, a novel monoclonal anti-PD-1 antibody. *Blood* 116: 2286–2294.
30. Moll, M., C. Kuylenstierna, V. D. Gonzalez, S. K. Andersson, L. Bosnjak, A. Sönnerborg, M. F. Quigley, and J. K. Sandberg. 2009. Severe functional impairment and elevated PD-1 expression in CD1d-restricted NKT cells retained during chronic HIV-1 infection. *Eur. J. Immunol.* 39: 902–911.
31. Pedicord, V. A., W. Montalvo, I. M. Leiner, and J. P. Allison. 2011. Single dose of anti-CTLA-4 enhances CD8+ T-cell memory formation, function, and maintenance. *Proc. Natl. Acad. Sci. USA* 108: 266–271.
32. Krummel, M. F., and J. P. Allison. 1996. CTLA-4 engagement inhibits IL-2 accumulation and cell cycle progression upon activation of resting T cells. *J. Exp. Med.* 183: 2533–2540.
33. Walunas, T. L., C. Y. Bakker, and J. A. Bluestone. 1996. CTLA-4 ligation blocks CD28-dependent T cell activation. *J. Exp. Med.* 183: 2541–2550.
34. Wang, W., D. Yu, A. A. Sarnaik, B. Yu, M. Hall, D. Morelli, Y. Zhang, X. Zhao, and J. S. Weber. 2012. Biomarkers on melanoma patient T cells associated with ipilimumab treatment. *J. Transl. Med.* 10: 146.
35. Nagata, S., T. Ise, and I. Pastan. 2009. Fc receptor-like 3 protein expressed on IL-2 nonresponsive subset of human regulatory T cells. *J. Immunol.* 182: 7518–7526.
36. Kochi, Y., R. Yamada, A. Suzuki, J. B. Harley, S. Shirasawa, T. Sawada, S. C. Bae, S. Tokuhiro, X. Chang, A. Sekine, et al. 2005. A functional variant in FCRL3, encoding Fc receptor-like 3, is associated with rheumatoid arthritis and several autoimmunities. *Nat. Genet.* 37: 478–485.
37. Ribas, A., B. Comin-Anduix, B. Chmielowski, J. Jalil, P. de la Rocha, T. A. McCannel, M. T. Ochoa, E. Seja, A. Villanueva, D. K. Oseguera, et al. 2009. Dendritic cell vaccination combined with CTLA4 blockade in patients with metastatic melanoma. *Clin. Cancer Res.* 15: 6267–6276.
38. Dhodapkar, K. M., S. N. Gettinger, R. Das, H. Zebroski, and M. V. Dhodapkar. 2013. SOX2-specific adaptive immunity and response to immunotherapy in non-small cell lung cancer. *OncoImmunology* 2: e25205.
39. Beck, K. E., J. A. Blansfield, K. Q. Tran, A. L. Feldman, M. S. Hughes, R. E. Royal, U. S. Kammula, S. L. Topalian, R. M. Sherry, D. Kleiner, et al. 2006. Enterocolitis in patients with cancer after antibody blockade of cytotoxic T-lymphocyte-associated antigen 4. *J. Clin. Oncol.* 24: 2283–2289.
40. Dinarello, C. A., and J. W. van der Meer. 2013. Treating inflammation by blocking interleukin-1 in humans. *Semin. Immunol.* 25: 469–484.